Mycobacterium tuberculosis protein tyrosine phosphatase (PtpA) excludes host vacuolar-H^+–ATPase to inhibit phagosome acidification

Dennis Wong, Horacio Bach, Jim Sun, Zakaria Hmama, and Yossef Av-Gay[1]

Department of Medicine, Division of Infectious Diseases, University of British Columbia, Vancouver, BC, Canada V5Z 3J5

Edited by Carl F. Nathan, Weill Medical College of Cornell University, New York, NY, and approved October 21, 2011 (received for review June 8, 2011)

Mycobacterium tuberculosis **(Mtb) pathogenicity depends on its ability to inhibit phagosome acidification and maturation processes after engulfment by macrophages. Here, we show that the secreted Mtb protein tyrosine phosphatase (PtpA) binds to subunit H of the macrophage vacuolar-H^+-ATPase (V-ATPase) machinery, a multisubunit protein complex in the phagosome membrane that drives luminal acidification. Furthermore, we show that the macrophage class C vacuolar protein sorting complex, a key regulator of endosomal membrane fusion, associates with V-ATPase in phagosome maturation, suggesting a unique role for V-ATPase in coordinating phagosome–lysosome fusion. PtpA interaction with host V-ATPase is required for the previously reported dephosphorylation of VPS33B and subsequent exclusion of V-ATPase from the phagosome during Mtb infection. These findings show that inhibition of phagosome acidification in the mycobacterial phagosome is directly attributed to PtpA, a key protein needed for Mtb survival and pathogenicity within host macrophages.**

phagocytosis | vesicular trafficking

The etiological agent of tuberculosis (TB), *Mycobacterium tuberculosis*, is one of the most devastating infectious agents in the world. One-third of the world's population is exposed to Mtb, which causes nearly 3 million deaths annually, and is expected to cause an estimated 1 billion new infections by 2020 (1). Mtb primarily infects alveolar macrophages that provide the first line of defense against microbial invasion. Normally, macrophages' engulfment of foreign bodies results in the formation of phagosome, which matures in a process that remodels its membrane and luminal contents through interaction and fusion with the endosomal network (2, 3). These membrane fusions allow the phagosome to acquire antimicrobial properties, including a profoundly acidic lumen, the hallmark of the macrophage maturation process (4).

Macrophages acidify the phagosomal lumen by recruiting V-ATPase, a multisubunit protein-pump complex that actively transports protons across membranes using energy from ATP hydrolysis (5). Structurally similar to ATP synthase, the V-ATPase consists of a membrane-bound domain with five different subunits and a cytosolic domain composed of subunits A–H (reviewed in ref. 6). Delivery of the V-ATPase to the phagosome results in a pH decrease from 6.5 to 5.0 within minutes of phagosome maturation (7). This acidic environment inhibits bacterial growth and enhances the activities of antimicrobial hydrolases. Acidic pH is also crucial for proper vesicular trafficking, directing the fusion of phagosomes with lysosomes or vesicles harboring antimicrobial molecules (8). Therefore, phagosome acidification is a critical event that prompts the destruction of invading particles into constituents for antigen presentation and the initiation of adaptive immune responses (9).

Intracellular pathogens that enter host cells through the phagocytic or endocytic pathway have developed mechanisms to counter the acidic environment within phagosomes. For instance, *Salmonella enterica* adapts to lower pH by activating acid tolerance genes (10). *Yersinia pseudotuberculosis* blocks phagosome acidification by directly inhibiting V-ATPase activity in mouse macrophages (11), and *Legionella pneumophila* secretes substrates into the host phagocyte to inhibit vacuole acidification through interaction with V-ATPase subunit A (12). In the case of Mtb, lack of acidification in the mycobacterial phagosome is mainly because of the absence of the V-ATPase on the phagosomal membrane (13). However, the mechanism by which Mtb accomplishes this remains undefined.

Mtb is known to be capable of sensing engulfment by macrophages and subsequently interferes with host signaling pathways to promote its intracellular survival (14–16). Mtb possesses a wide repertoire of signal transduction systems, including 11 two-component systems, 11 eukaryotic-like serine/threonine protein kinases (PknA-PknL), two protein tyrosine phosphatases (PtpA and PtpB), and the newly identified protein tyrosine kinase (PtkA) (17–19). These signaling proteins play key roles in bacterial adaptation and response to host defense mechanisms. PtpA, a secreted protein phosphatase, is essential for Mtb pathogenicity, participating in the arrest of phagosome maturation within the host macrophages (14, 20). Earlier, we identified the host vacuolar protein sorting 33B (VPS33B) as the cognate substrate of PtpA (18). VPS33B is a member of the class C VPS complex that regulates membrane fusion within the endocytic pathway (21). PtpA dephosphorylation of VPS33B inactivates this host protein, leading to inhibition of phagosome–lysosome fusion (14).

In this work, we report that Mtb PtpA binds to subunit H of macrophage V-ATPase to block V-ATPase trafficking and phagosome acidification. We further identified a unique role for V-ATPase in the process of phagosome–lysosome fusion. Our results demonstrated that Mtb success in inhibiting phagosome acidification and establishing infection in host macrophages relies on PtpA.

Results

Mtb PtpA Binds Subunit H of Human V-ATPase. Previously, we used a substrate-trapping mutant of PtpA to pull down the catalytic substrate of PtpA, VPS33B, from the Mtb-infected THP-1 cell lysate (14). Interestingly, when we used the WT recombinant PtpA as bait, we were able to pull down another, previously unidentified, 55-kDa macrophage protein (14). We identified this protein by MALDI-TOF mass spectrometry to be subunit H of human V-ATPase (Fig. S1*A*) and verified its identity by Western blot analysis (Fig. 1*A*). In vitro kinase assay and phosphoamino acid analysis showed that subunit H was phosphorylated on threonine and could not serve as a catalytic substrate for the tyrosine phosphatase PtpA (Fig. S1 *B* and *C*). In vitro protein–protein interaction analysis of PtpA and subunit H demonstrated direct contact between mycobacterial PtpA and host V-ATPase subunit H (Fig. 1 *B* and *C*). A hyperbolic curve fitting

Author contributions: D.W., H.B., Z.H., and Y.A.-G. designed research; D.W. and J.S. performed research; D.W., Z.H., and Y.A.-G. analyzed data; and D.W. and Y.A.-G. wrote the paper.

The authors declare no conflict of interest.

This article is a PNAS Direct Submission.

[1]To whom correspondence should be addressed. E-mail: yossi@interchange.ubc.ca.

This article contains supporting information online at www.pnas.org/lookup/suppl/doi:10.1073/pnas.1109201108/-/DCSupplemental.

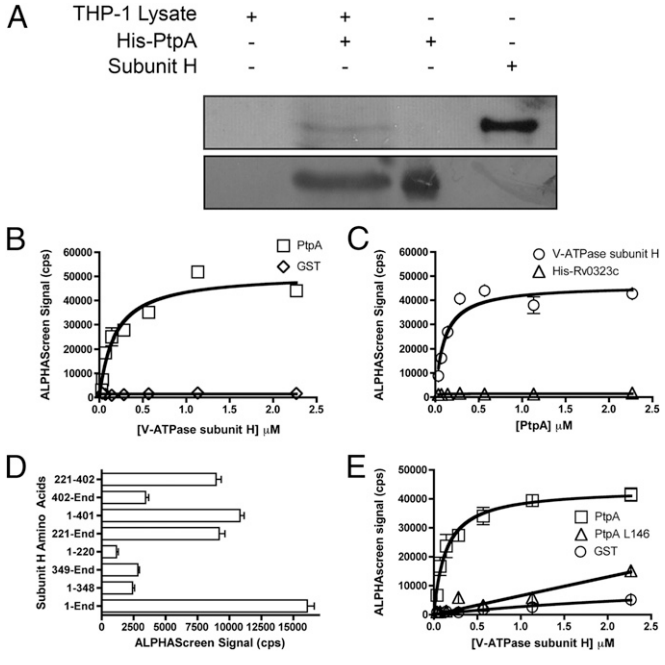

Fig. 1. PtpA interacts with the V-ATPase subunit H in vitro. (*A*) In vitro pull-down using recombinant His-tagged Mtb PtpA captured human V-ATPase subunit H from THP-1 macrophage lysate. The eluates were analyzed on Western blots using rabbit anti-subunit H and anti-PtpA antibodies. (*B*) Recombinant PtpA was subjected to an ALPHAScreen assay with increasing concentration of V-ATPase subunit H. GST served as negative control. Curve fitting yielded K_d 1.1×10^{-7} M. (*C*) The reciprocal experiment with increasing PtpA concentration yielded similar results. His-tagged Rv0323c protein was used as negative control. (*D*) Mapping of the PtpA binding site on V-ATPase subunit H. Overlapping truncated recombinant subunit H protein fragments were incubated with recombinant PtpA proteins in an ALPHAScreen assay. Amino acid 220–402 of subunit H is the minimal region required for binding PtpA. (*E*) Site-directed mutagenesis generated a recombinant mutant PtpA protein ($PtpA^{L146A}$) that failed to interact with subunit H.

the 1:1 Langmuir binding model and a dissociation constant of K_d 1.1×10^{-7} M indicate a high level of affinity between the two proteins.

PtpA Binds to Amino Acids 220–402 of Subunit H. We determined the PtpA binding site on subunit H by constructing overlapping polypeptide fragments of subunit H. As shown in Fig. 1*D*, only fragments that included the linker region (amino acid 220–402) were able to bind PtpA with high affinity. This finding is consistent with previous predictions that the linker region of subunit H is involved in protein–protein interactions (22).

The C-Terminal α-Helix of PtpA Binds Subunit H. Subunit H was reported to interact with dileucine-based motifs on the HIV Nef protein (23). Therefore, we performed site-directed mutagenesis to investigate whether dileucine motifs or other leucine residues on PtpA participate in binding subunit H (Fig. S2*A*). One mutant, $PtpA^{L146A}$, located in the C-terminal α-helix, was defective in binding subunit H (Fig. 1*E*). This finding and the previous findings are consistent with the predicted structure of PtpA bound to subunit H using the protein-docking algorithm 3D-Garden (Fig. S2 *B* and *C*) (24). Interestingly, the $PtpA^{L146A}$ mutant retained its phosphatase activity with kinetics similar to the WT protein (Fig. S2*D*). This result is in line with our observation that subunit H is not a catalytic substrate but rather a binding partner of PtpA.

PtpA Binds V-ATPase Subunit H in Vivo. Using immunoprecipitation, we investigated the in vivo interaction between PtpA and subunit H during macrophage infection. Antibodies against subunit H coimmunoprecipitated PtpA from lysates of THP-1 cells infected with H37Rv Mtb expressing WT PtpA, confirming the physiological relevance of PtpA/subunit H interaction during Mtb infection (Fig. 2*A*).

To further monitor PtpA interaction with subunit H, we used a modified split-Trp mycobacterial assay for detecting protein–protein interactions (25, 26). In this system, a tryptophan auxotrophic strain of *Mycobacterium smegmatis* only grows in the absence of tryptophan if the tested proteins interact with each other. As shown in Fig. 2*B*, coexpression of subunit H and PtpA fusion proteins restored mycobacterial growth on 7H9 agar plates, confirming protein–protein interaction within a surrogate host. Coexpression with the binding-defective $PtpA^{L146A}$ did not lead to mycobacterial growth, suggesting that this phosphatase-active PtpA mutant lost its ability to bind subunit H. The phosphatase-defective $PtpA^{D126A}$ retained its subunit H binding ability, further indicating the interaction is independent of the catalytic activity of PtpA (Fig. 2*B*).

PtpA Binding to Subunit H Is Required for Mtb Intracellular Survival. To test whether PtpA binding to subunit H is required for Mtb pathogenicity, we investigated the ability of the binding-defective $PtpA^{L146A}$ Mtb strain to survive in human THP-1 macrophages. As shown in Fig. 2*C*, a Δ*ptpA* strain complemented with a construct encoding $PtpA^{L146A}$ was attenuated within the macrophage in a manner similar to that of the Δ*ptpA* knockout strain, whereas the parental and the complement strains were able to establish a stable infection after 3 d. Expression and stability of the WT and mutant PtpA proteins in these strains were confirmed with Western blot analysis (Fig. S3*A*). At 6 d after infection, the binding-defective strain showed a 2-log reduction in cfu compared with the WT strain. Though the parental and complemented strains entered into growth phase within the macrophage, the Δ*ptpA* and the binding-defective strains were continually cleared, establishing the importance of PtpA interaction with the V-ATPase machinery for Mtb survival within macrophages.

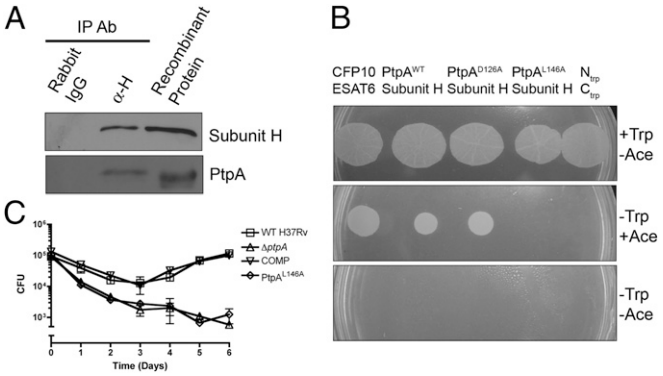

Fig. 2. PtpA and V-ATPase subunit H interacts in vivo. (*A*) PtpA coimmunoprecipitated with subunit H from THP-1 macrophages infected with Mtb-expressing PtpA. Immunoprecipitation (IP) was performed with either rabbit anti-subunit H (α-H) antibodies (Ab) or rabbit IgG as negative control. (*B*) PtpA and subunit H interacted in the split-Trp protein fragment complementation assay to facilitate N_{trp} and C_{trp} reassembly required for Trp biosynthesis, thus enabling growth of the *M. smegmatis* *Trp*$^-$ strain coexpressing N_{trp}-PtpA and subunit H-C_{trp} under acetamide (ACE) induction (*Middle*). N_{trp}-$PtpA^{L146A}$ failed to interact with subunit H-C_{trp} to restore *M. smegmatis* growth. N_{trp}-ESAT6 and CFP10-C_{trp} were used as a positive control. The negative control consisted of N_{trp} and C_{trp} fragments alone. (*Top*) Transformed strains are capable of growing on Trp-supplemented media. (*Bottom*) No growth is observed in the absence of acetamide induction and exogenous Trp. (*C*) Loss of PtpA binding to V-ATPase subunit H impairs Mtb survival within host macrophages. V-ATPase binding-defective $PtpA^{L146A}$-expressing Mtb strain showed a 2-log reduction in bacterial load compared with the WT strain at 6 d postinfection.

PtpA Inhibits Phagosome Acidification. The in vivo PtpA/subunit H interaction and the impaired intracellular survival of the binding-defective PtpA^{L146A} strain suggest that PtpA interferes with the phagosome acidification process. To examine this hypothesis, we used FACS to analyze the pH of Mtb-containing phagosomes. Parental and mutant strains were dually labeled with the pH-sensitive pHrodo fluorescent dye and the pH-insensitive Alexa Fluor 488 while undergoing phagocytosis by THP-1 macrophages. Covalent labeling of the bacteria with fluorescent dyes does not affect PtpA secretion (Fig. S3*B*). Overlaid FACS histograms showed a clear increase in the mean pHrodo fluorescence intensity for phagosomes harboring Δ*ptpA* Mtb, Δ*ptpA* complemented with the phosphatase-inactive *ptpA*^{D126A}, and Δ*ptpA* complemented with the binding-defective *ptpA*^{L146A} (corresponding to pH 5.8, 5.6, and 5.55, respectively), compared with phagosome containing parental and complemented Mtb (corresponding to pH 6.7 and 6.4, respectively) (Fig. 3 *A* and *B*, Fig. S4, and Table S1). These results indicate a direct functional role for PtpA in the inhibition of Mtb phagosome acidification, which is dependent on both the binding ability and phosphatase activity of PtpA.

To examine PtpA's ability to modulate phagosome acidification independently of other Mtb proteins, we transfected THP-1 macrophages with GFP-fused constructs of parental and mutated forms of PtpA in a mammalian vector. All constructs were expressed at similar levels, and the survival and phagocytic ability of the macrophages were not impaired by the transfection (Fig. S5 *A* and *B*). PtpA-transfected macrophages were infected with *Escherichia coli* labeled with pHrodo and Alexa Fluor 350, and the phagosomal pH was assessed by spectrofluorometry (Fig. S5*C*). Expression of PtpA within THP-1 macrophages inhibited acidification of *E. coli*-containing phagosomes, whereas both catalytically inactive PtpA^{D126A} and binding mutant PtpA^{L146A} were unable to block phagosome acidification, showing a marked decrease in phagosomal pH similar to untransfected and empty vector control macrophages (Fig. 3*C*). Digital confocal microscopy of the infected macrophages confirmed these findings (Fig. 3*D* and Fig. S5*D*). These results established that PtpA alone can effectively prevent phagosome acidification in the macrophage. This inhibition depends on both PtpA phosphatase activity and its ability to bind to host V-ATPase machinery.

V-ATPase Machinery Recruits the Class C VPS Complex. The interaction of PtpA with both subunit H and the previously described VPS33B (14) suggested that the V-ATPase and class C VPS complexes might be in close proximity or even directly interact during phagosome maturation and endosome–lysosome fusion. To investigate this hypothesis, we conducted immunoprecipitation experiments in THP-1 macrophages using antibodies against VPS33B as bait and probed for subunits H, B, and E of the V-ATPase complex and VPS18 of the class C VPS complex by Western blot. In uninfected THP-1 macrophages, faint bands corresponding to subunits of the V-ATPase complex were captured with VPS33B and VPS18 when a higher amount of lysate was used (Fig. S6*A*). This finding suggests that V-ATPase interacts transiently with the class C VPS to regulate normal endosome–lysosome fusion in resting cells. Furthermore, this interaction is up-regulated upon phagocytosis of *E. coli*, as demonstrated by the prominent bands of V-ATPase subunits captured 2 h postinfection (Fig. 4*A* and Fig. S6*A*), further supporting that the class C VPS complex interaction with V-ATPase has a key role in phagosome maturation and fusion with lysosome.

Mtb PtpA Blocks the Interaction Between Class C VPS and V-ATPase Complexes. When THP-1 macrophages were infected with Mtb H37Rv, subunit H, B, or E of the V-ATPase machinery was not captured using antibodies against VPS33B (Fig. 4*A*). Mtb inhibition of V-ATPase and class C VPS interaction is maintained 24 h postinfection (Fig. S6*B*). However, the V-ATPase subunits coimmunoprecipitated with VPS33B and VPS18 in THP-1 macrophages infected with Δ*ptpA*. Complementation of the Δ*ptpA* mutant strain with WT *ptpA* restored the ability of Mtb to inhibit class C VPS interaction with the V-ATPase complex. Furthermore, complementation with *ptpA*^{D126A}, but not *ptpA*^{L146A}, restored Mtb inhibition of class C VPS and V-ATPase interaction (Fig. 4*A*). These results indicate that Mtb infection disrupted the V-ATPase and class C VPS association; PtpA is responsible for blocking this interaction; and PtpA binding to subunit H is specifically necessary for this disruption.

VPS33B Remains Phosphorylated in THP-1 Macrophages Infected with Binding-Defective PtpA. VPS33B phosphorylation is required for phagosome–lysosome fusion, and Mtb PtpA dephosphorylation of VPS33B blocks this process (14). Because the class C VPS complex is recruited to the V-ATPase, we asked whether PtpA

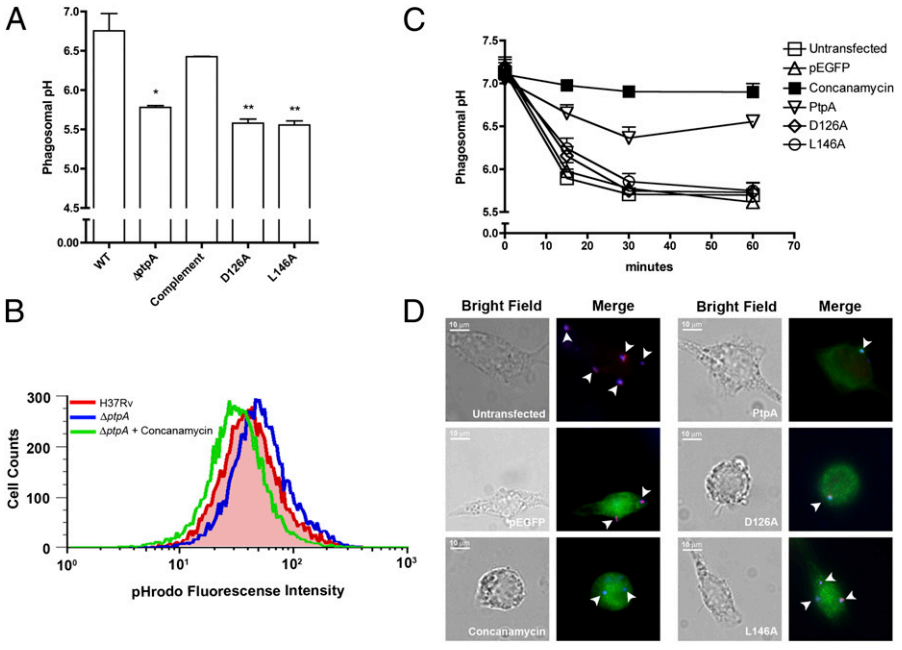

Fig. 3. Mtb PtpA inhibits phagosome acidification. (*A*) The indicated Mtb strains were labeled with pH-sensitive fluorescent dye (pHrodo) and used to infect THP-1 macrophages. Phagosomal pH of the infected macrophages was measured with FACS. WT Mtb maintained a phagosomal pH of ~6.7, whereas phagosomes of both Δ*ptpA* and PtpA^{L146A} strains were acidified to ~pH 5.5. **P* < 0.05; ***P* < 0.01 (significant difference compared with H37Rv by Student *t* test). (*B*) Overlaid FACS histograms of the pHrodo fluorescence intensity of the WT H37Rv and Δ*ptpA* phagosomes show a shift in phagosomal pH in the presence of PtpA. (*C*) THP-1 macrophages were transfected with GFP-tagged constructs of WT and mutant PtpA proteins and infected with pHrodo-labeled *E. coli*. Phagosomal pH was measured with spectrofluorometry during the course of infection. WT PtpA inhibits *E. coli* phagosome acidification (pH 6.5), whereas the binding-defective PtpA^{L146A} failed to block acidification (pH 5.6). Concanamycin was added as a positive control for inhibition of phagosome acidification. (*D*) Digital confocal microscopy of the infected macrophages in *C* confirms the inhibition of phagosome acidification by Mtb PtpA. Green, expression of GFP or GFP-tagged PtpA constructs; red, pHrodo fluorescence in acidified phagosomes; blue, Alexa Fluor 350-labeled *E. coli*.

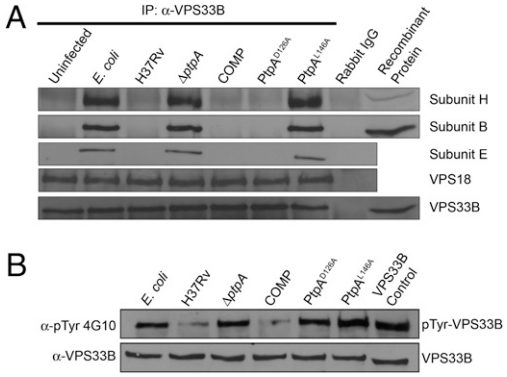

Fig. 4. Mtb PtpA disrupts the interaction between the class C VPS and V-ATPase complexes during infection. Immunoprecipitation was performed with anti-VPS33B (α-VPS33B) using 2 mg of soluble lysate from THP-1 macrophages infected with the indicated strain for 2 h and followed by Western blot analysis with the indicated antibody. Rabbit IgG was used as negative control. (*A*) The class C VPS (VPS33B and VPS18) interacts with the V-ATPase complexes (subunits B, H, and E) from THP-1 macrophages infected with *E. coli*, Δ*ptpA*, and PtpA^{L146A}. The parental H37Rv, PtpA^{D126A}, and the complemented strain disrupted the host proteins interaction. (*B*) Western blot analysis of VPS33B phosphorylation in vivo. VPS33B remained phosphorylated in macrophages infected with the PtpA^{L146A}-expressing strain. (*Upper*) Probed with antiphosphotyrosine antibody 4G10. (*Lower*) Probed with anti-VPS33B to ensure equal loading.

binding to V-ATPase subunit H affects the phosphorylation status of VPS33B during Mtb infection. To address this question, we immunoprecipitated VPS33B and analyzed its phosphorylation with the antiphosphotyrosine antibody 4G10. When *E. coli* was used to infect macrophages, VPS33B was phosphorylated (Fig. 4*B*). However, as expected, when macrophages were infected with Mtb, down-regulation of VPS33B phosphorylation was observed. The Δ*ptpA* strain did not reduce VPS33B phosphorylation, and this was reversed by complementation with WT *ptpA*. Interestingly, VPS33B remained phosphorylated in macrophages infected with Δ*ptpA* complemented with either the phosphatase-defective *ptpA*^{D126A} or the binding-defective *ptpA*^{L146A}, despite being catalytically active (Fig. 4*B*). This finding suggests that the binding of PtpA to subunit H of V-ATPase is a prerequisite for VPS33B dephosphorylation, which is consistent with our findings that the loss of interaction with subunit H renders PtpA nonfunctional within the host cell.

PtpA Binding to Subunit H Participates in the Exclusion of the V-ATPase from the Mtb Phagosome. Disruption of the interaction between class C VPS and V-ATPase by PtpA suggests that PtpA directly impairs V-ATPase trafficking to the Mtb phagosome. To check the effect of PtpA on V-ATPase trafficking, we used digital confocal microscopy to monitor class C VPS and V-ATPase localization within infected macrophages, represented by VPS33B and subunit H, respectively. As illustrated in Fig. 5*A*, VPS33B and V-ATPase subunit H colocalized to the phagosome of macrophages infected with *E. coli*. In contrast, whereas Mtb-infected macrophage phagosomes were decorated with VPS33B, subunit H was excluded, indicating a lack of V-ATPase recruitment. However, the Δ*ptpA* knockout strain exhibited colocalization of VPS33B and subunit H on the mycobacterial phagosomal membrane. Complementation with WT *ptpA* reversed this pattern with a similar percentage of phagosomes lacking V-ATPase as the WT strain (Fig. 5*B*). Corecruitment of subunit H and VPS33B to the bacilli-containing phagosomes was not observed despite complementation with either the catalytically inactive *ptpA*^{D126A} or the binding-defective *ptpA*^{L146A}. Therefore, PtpA binding to subunit H is needed for blocking V-ATPase trafficking to the Mtb phagosome, leading to the inhibition of Mtb phagosome acidification.

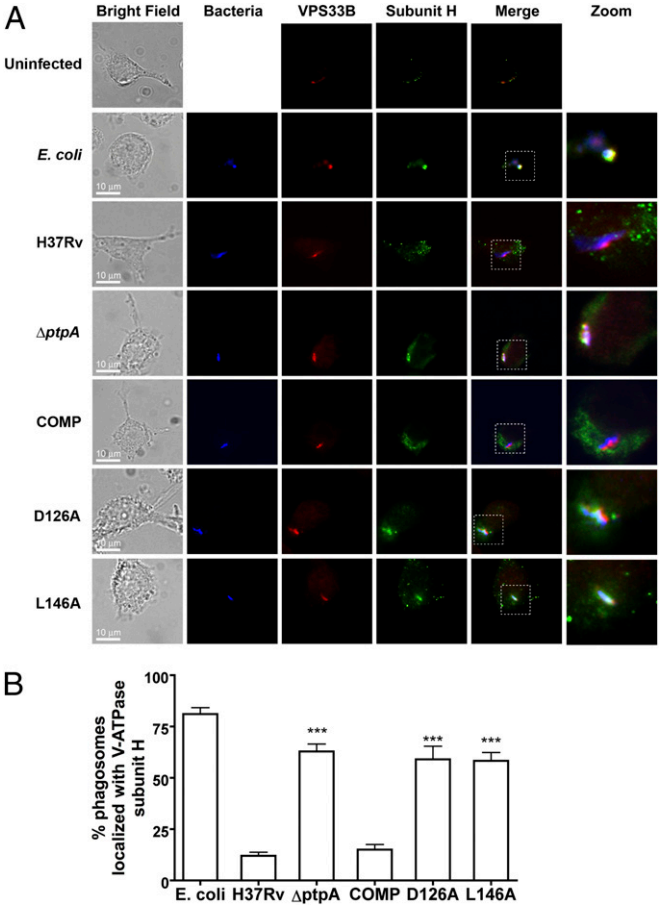

Fig. 5. Confocal microscopy of THP-1 macrophages infected with *E. coli* or indicated Mtb strains. (*A*) Localization of VPS33B and V-ATPase subunit H was detected with immunofluorescence staining. V-ATPase was excluded from the Mtb phagosome in macrophages infected with the WT strain, whereas the Δ*ptpA* phagosome acquired V-ATPase. The phagosomes of the binding-defective PtpA^{L146A}-expressing strain also failed to exclude host V-ATPase. (*B*) Quantification of the confocal data shown in *A*. Values are the mean ± SD of phagosome colocalization with V-ATPase subunit H in 50–80 cells from three independent experiments. ***$P < 0.001$ (significant difference compared with H37Rv by Student *t* test).

Although we have shown that the antibodies against VPS33B and subunit H are highly specific (Fig. S7), to overcome any potential cross-reactivity, we also performed double transfection of the THP-1 macrophages with GFP and DsRed2-fused constructs of subunit H and VPS33B, respectively, allowing direct visualization of host proteins' localization within the macrophage. Colocalization of GFP-subunit H and DsRed2-VPS33B in uninfected macrophages provides further support that V-ATPase and class C VPS functions in the same pathway to regulate normal endosome–lysosome fusion. When the transfected macrophages were infected with the same Mtb strains, similar patterns of subunit H and VPS33B localization was observed compared with the immunofluorescent-stained macrophages (Fig. S8). This result further supports that PtpA binding to subunit H is needed for the exclusion of V-ATPase from the phagosome.

Discussion

More than a decade ago, Sturgill-Koszycki et al. (13) showed that macrophages fail to acidify phagosomes containing mycobacteria because these phagosomes did not accumulate the V-ATPase responsible for phagosomal acidification. This finding suggested inhibition of the fusion between membrane vesicles harboring

the V-ATPase complex and the mycobacterial phagosome (13). Despite the lack of a mechanistic explanation, the exclusion of the V-ATPase complex during Mtb infection has become a long-established paradigm. Here, we show that the lack of phagosome acidification is directly attributed to the Mtb-secreted protein PtpA, which specifically inhibits V-ATPase trafficking to the mycobacterial phagosome during phagosome maturation.

The exact mechanism by which PtpA is secreted across the phagosomal membrane remains unclear. However, using electron microscopy, neutralizing antibodies, and Western blot analysis, we have previously shown that PtpA is present in the host cytosol milieu (14, 27). There is evidence suggesting that bacterial proteins <70 kDa in molecular size can cross the phagosomal membrane (28). This observation might be related to the more recent discovery that the ESX-1 secretion system with its substrate ESAT-6 can activate the inflammasome and perturb host cell membrane to facilitate the translocation of mycobacterial proteins into the macrophage cytosol (29, 30). Further investigation is needed to elucidate the mechanistic details of PtpA secretion.

We have shown previously that Mtb PtpA dephosphorylates the host macrophage protein VPS33B, a key regulator of membrane fusion, leading to inhibition of phagosome–lysosome fusion (14). In this study, we identified an additional key partner to the process, subunit H of the host V-ATPase machinery. The interaction with V-ATPase subunit H and dephosphorylation of VPS33B are both required for PtpA inhibition of macrophage phagosome–lysosome fusion and phagosome acidification. We were able to identify a catalytically active mutant, $PtpA^{L146A}$, which does not interact with subunit H. Because of its predicted location within the core region of PtpA (Fig. S2 *A* and *B*), this mutation most likely alters the conformation of the entire C-terminal α-helix, leading to defective binding. The loss of either PtpA phosphatase activity or subunit H binding renders PtpA nonfunctional within the host cell.

During phagosome maturation, lysosomal V-ATPase is directly recruited to the phagosomal membrane for luminal acidification (3). The class C VPS complex has been implicated in this process as the membrane-tethering factor. Although studies of *Drosophila* neurons and mammalian renal medulla cells have shown interaction between subunits of V-ATPase and SNARE proteins (31, 32), our studies of PtpA in Mtb demonstrate a direct interaction between the class C VPS and V-ATPase. We further showed that this mechanism is not limited to phagosome maturation, because the same interaction could be detected, albeit at a weaker level, in uninfected macrophages. This finding suggests that class C VPS and V-ATPase interacts transiently in the resting cell to regulate normal endosome–lysosome fusion, and this association is likely up-regulated during phagocytosis to deliver lysosomal contents to the phagosome. Our finding provides compelling evidence that V-ATPase is a key player in the membrane fusion machinery, particularly in cooperating with the class C VPS complex to tether the fusing phagosomal or endosomal membrane with the lysosome (Fig. 6). Disruption by Mtb PtpA further exemplifies the importance of this interaction in host defense mechanism.

With these results, our current model suggests a two-step process for PtpA exclusion of V-ATPase and inactivation of VPS33B. During Mtb infection, PtpA binding to subunit H may first disrupt initial membrane tethering and localize it to the proximity of its catalytic substrate VPS33B (Fig. 6). Subsequent dephosphorylation of VPS33B would then inactivate the entire membrane fusion machinery and its downstream effectors, preventing delivery of V-ATPase to the mycobacterial phagosome. This mechanism would explain the failure of the phosphatase-defective mutant $PtpA^{D126A}$, which retains the capability of binding to V-ATPase and disrupting host complex associations, to shut down the host macrophage pathway completely. Our observation that VPS33B remains phosphorylated in both the phosphatase-defective and binding-defective strain supports such a two-step process, suggesting that PtpA binding to subunit H is a prerequisite for VPS33B dephosphorylation. This phenomenon is also supported by our confocal data, where both the $PtpA^{D126A}$ and $PtpA^{L146A}$ strains failed to inhibit V-ATPase trafficking to Mtb phagosomes.

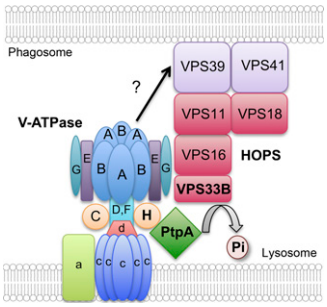

Fig. 6. A model for the specific exclusion of V-ATPase and the inhibition of mycobacterial phagosome acidification by PtpA. During infection, the V-ATPase recruits the class C VPS complex, possibly associated with VPS39 and VPS41 as the HOPS complex, aiding the tethering of the fusing phagosomal and lysosomal membranes. PtpA, secreted into the host cytosol by Mtb, binds to subunit H of the V-ATPase complex, disrupting the interaction between the two protein complexes and localizing itself near its catalytic substrate, VPS33B. PtpA then dephosphorylates and inactivates VPS33B, thereby shutting down the membrane fusion machinery. Binding to subunit H, therefore, allows PtpA to specifically inhibit V-ATPase trafficking to the mycobacterial phagosome.

However, the mycobacterial phagosome is not an isolated compartment; rather, it interacts extensively with early endosome to acquire nutrients, such as iron-bound transferrin, to maintain survival within the host cell (33). Vesicle fusion in the endocytic pathway depends on two membrane-tethering protein complexes, class C core vacuole/endosome tethering (CORVET) and homotypic fusion and protein sorting (HOPS) (34, 35). The class C VPS complex serves as the core of both CORVET and HOPS complexes through reversible association with CORVET-specific (VPS3 and VPS8) and HOPS-specific (VPS39 and VPS41) accessory subunits, which mediate early-to-late endosome fusion events and fusions with lysosome, respectively (reviewed in ref. 36). Our results suggest that V-ATPase may specifically interact with the HOPS complex during phagosome–lysosome fusion (Fig. 6). Therefore, by binding to the V-ATPase, PtpA could specifically localize to the phagosome–lysosome interface, and CORVET-mediated early endosome fusions with the phagosome will remain intact. This specific localization mechanism would then allow PtpA to distinguish HOPS from CORVET, thereby specifically excluding V-ATPase to inhibit mycobacterial phagosome acidification. In fact, a link between the V-ATPase and HOPS complexes was observed by a previous study demonstrating that the HOPS-specific subunit VPS41 failed to function in yeast that had mutations in the V-ATPase complex (37). This finding suggests that the HOPS-specific subunits VPS39 and VPS41 might be direct effectors of the V-ATPase complex during phagosome–lysosome fusion (Fig. 6), and the CORVET complex might be recruited to the phagocytic pathway through a different mechanism. As the HOPS-specific subunits are known to interact with activated Rab7 during endosome maturation (38), it is likely that Rab7 is the upstream activator of V-ATPase association with class C VPS complex. Further experiments will be needed to fully characterize these host cellular pathways in the context of mycobacterial infection. Nonetheless, our study clearly demonstrates that the absence of V-ATPase and the lack of mycobacterial phagosome acidification are directly attributed to the Mtb protein tyrosine phosphatase PtpA.

Materials and Methods

In Vitro Pull-Down Assay. In vitro pull-down assay with recombinant His-tagged PtpA was performed as described previously (14).

ALPHAScreen Protein–Protein Interaction Assay. An assay using the ALPHAScreen Histidine (Nickel Chelate) Detection Kit was performed according to the manufacturer's protocol (Perkin-Elmer). Purified recombinant protein was biotinylated using the EZ-Link Biotinylation Kit (Pierce) according to the manufacturer's protocol.

Mycobacterial Split-Trp Protein–Protein Interaction Assay. DNA encoding PtpA and subunit H were cloned into pJC10 and pJC11 vectors, generating translational fusion constructs with the N_{trp} and C_{trp} fragments, respectively, of the *N*-(5′-phosphoribosyl)-anthranilate isomerase under the control of the acetamidase promoter. The split-Trp assay (26) was carried out as described previously (25).

Infection of THP-1. THP-1 human-derived monocytes (ATCC; TIB-202) were grown in RPMI medium 1640 (Sigma) supplemented with 10% FBS, 1% L-glutamine (StemCell). THP-1 cells (1.0×10^6 or 5.0×10^5) were seeded onto 12- or 24-well tissue culture plates, respectively, and differentiated with 40 ng/mL 12-phorbol 13-myristate acetate in RPMI 1640 supplemented with 10% FBS and 1% L-glutamine. Infection of THP-1 macrophages was performed using human serum-opsonized Mtb or *E. coli* DH5α at a multiplicity of infection (MOI) of 10:1. For Mtb intracellular survival studies, infected macrophages (MOI 1:1) were harvested at defined time points, lysed with 0.025% SDS, serial diluted, and plated on 7H10 agar medium supplemented with appropriate antibiotics.

Immunofluorescence Microscopy. THP-1 macrophages were seeded on coverslips at 5.0×10^5 cells/well in 24-well tissue culture plates. Infection of THP-1 macrophages and immunostaining was performed as described previously (14, 39) (more details in *SI Materials and Methods*).

Measurement of Phagosomal pH. Assessment of the phagosomal pH of *E. coli* and Mtb phagosomes was performed according to previous literature (40, 41). Bacteria were labeled with the pH-sensitive pHrodo probe (Invitrogen), which emits red fluorescence in acidic environment, and the indicated pH-insensitive probes [Alexa Fluor 350 (Blue) and Alexa Fluor 488 (Green); Invitrogen] according to established protocols (41). Phagosomal pH was measured with either spectrofluorometry in the Fusion-Alpha HT Microplate Reader (Perkin-Elmer) or with FACS in the FACSCalibur Flow Cytometer (BD Bioscience). The calculated fluorescence ratios of the pH-sensitive and pH-insensitive probes were used to determine phagosomal pH according to a calibration curve. pH calibration was performed by incubating infected THP-1 macrophages in 10 mM phosphate-citrate buffer of predetermined pH (5.0–8.0) containing 145 mM KCl, 1 mM $MgCl_2$, 0.5 mM $CaCl_2$, 10 mM glucose, 20 μM nigericin, and 4 μM monesin (Figs. S4 and S8). Concanamycin (50 nM) was added to the macrophages to inhibit V-ATPase proton transport in the indicated samples (more details in *SI Materials and Methods*).

ACKNOWLEDGMENTS. We thank the British Columbia Centre for Disease Control for providing access to a containment level 3 facility and Mary Ko and Joseph Chao for technical assistance. D.W. is a recipient of the Canadian Institutes of Health Research Canada Graduate Scholarships Doctoral Award. This study was funded by Canadian Institute of Health Research Operating Grant MOP-106622 (to Y.A.-G.).

1. Dye C, Williams BG (2010) The population dynamics and control of tuberculosis. *Science* 328:856–861.
2. Bright NA, Gratian MJ, Luzio JP (2005) Endocytic delivery to lysosomes mediated by concurrent fusion and kissing events in living cells. *Curr Biol* 15:360–365.
3. Sun-Wada GH, Tabata H, Kawamura N, Aoyama M, Wada Y (2009) Direct recruitment of H+-ATPase from lysosomes for phagosomal acidification. *J Cell Sci* 122:2504–2513.
4. Tjelle TE, Lovdal T, Berg T (2000) Phagosome dynamics and function. *Bioessays* 22: 255–263.
5. Hackam DJ, et al. (1997) Regulation of phagosomal acidification. Differential targeting of Na+/H+ exchangers, Na+/K+-ATPases, and vacuolar-type H+-atpases. *J Biol Chem* 272:29810–29820.
6. Forgac M (2007) Vacuolar ATPases: Rotary proton pumps in physiology and pathophysiology. *Nat Rev Mol Cell Biol* 8:917–929.
7. Mukherjee S, Ghosh RN, Maxfield FR (1997) Endocytosis. *Physiol Rev* 77:759–803.
8. van Deurs B, Holm PK, Sandvig K (1996) Inhibition of the vacuolar H(+)-ATPase with bafilomycin reduces delivery of internalized molecules from mature multivesicular endosomes to lysosomes in HEp-2 cells. *Eur J Cell Biol* 69:343–350.
9. Jutras I, Desjardins M (2005) Phagocytosis: At the crossroads of innate and adaptive immunity. *Annu Rev Cell Dev Biol* 21:511–527.
10. Prost LR, et al. (2007) Activation of the bacterial sensor kinase PhoQ by acidic pH. *Mol Cell* 26(2):165–174.
11. Tsukano H, et al. (1999) *Yersinia pseudotuberculosis* blocks the phagosomal acidification of B10.A mouse macrophages through the inhibition of vacuolar H(+)-ATPase activity. *Microb Pathog* 27:253–263.
12. Xu L, et al. (2010) Inhibition of host vacuolar H+-ATPase activity by a *Legionella pneumophila* effector. *PLoS Pathog* 6:e1000822.
13. Sturgill-Koszycki S, et al. (1994) Lack of acidification in Mycobacterium phagosomes produced by exclusion of the vesicular proton-ATPase. *Science* 263:678–681.
14. Bach H, Papavinasasundaram KG, Wong D, Hmama Z, Av-Gay Y (2008) *Mycobacterium tuberculosis* virulence is mediated by PtpA dephosphorylation of human vacuolar protein sorting 33B. *Cell Host Microbe* 3:316–322.
15. Hestvik AL, Hmama Z, Av-Gay Y (2003) Kinome analysis of host response to mycobacterial infection: A novel technique in proteomics. *Infect Immun* 71:5514–5522.
16. Hestvik AL, Hmama Z, Av-Gay Y (2005) Mycobacterial manipulation of the host cell. *FEMS Microbiol Rev* 29:1041–1050.
17. Av-Gay Y, Everett M (2000) The eukaryotic-like Ser/Thr protein kinases of *Mycobacterium tuberculosis*. *Trends Microbiol* 8:238–244.
18. Bach H, Wong D, Av-Gay Y (2009) *Mycobacterium tuberculosis* PtkA is a novel protein tyrosine kinase whose substrate is PtpA. *Biochem J* 420(2):155–160.
19. Chao J, et al. (2010) Protein kinase and phosphatase signaling in *Mycobacterium tuberculosis* physiology and pathogenesis. *Biochim Biophys Acta* 1804:620–627.
20. Cowley SC, Babakaiff R, Av-Gay Y (2002) Expression and localization of the *Mycobacterium tuberculosis* protein tyrosine phosphatase PtpA. *Res Microbiol* 153: 233–241.
21. Rieder SE, Emr SD (1997) A novel RING finger protein complex essential for a late step in protein transport to the yeast vacuole. *Mol Biol Cell* 8:2307–2327.
22. Sagermann M, Stevens TH, Matthews BW (2001) Crystal structure of the regulatory subunit H of the V-type ATPase of *Saccharomyces cerevisiae*. *Proc Natl Acad Sci USA* 98:7134–7139.
23. Geyer M, et al. (2002) Subunit H of the V-ATPase binds to the medium chain of adaptor protein complex 2 and connects Nef to the endocytic machinery. *J Biol Chem* 277:28521–28529.
24. Lesk VI, Sternberg MJ (2008) 3D-Garden: A system for modelling protein-protein complexes based on conformational refinement of ensembles generated with the marching cubes algorithm. *Bioinformatics* 24:1137–1144.
25. Chao JD, et al. (2010) Convergence of Ser/Thr and two-component signaling to coordinate expression of the dormancy regulon in *Mycobacterium tuberculosis*. *J Biol Chem* 285:29239–29246.
26. O'Hare H, Juillerat A, Dianisková P, Johnsson K (2008) A split-protein sensor for studying protein-protein interaction in mycobacteria. *J Microbiol Methods* 73(2): 79–84.
27. Bach H, Sun J, Hmama Z, Av-Gay Y (2006) *Mycobacterium avium* subsp. *paratuberculosis* PtpA is an endogenous tyrosine phosphatase secreted during infection. *Infect Immun* 74:6540–6546.
28. Teitelbaum R, et al. (1999) Mycobacterial infection of macrophages results in membrane-permeable phagosomes. *Proc Natl Acad Sci USA* 96:15190–15195.
29. Mishra BB, et al. (2010) *Mycobacterium tuberculosis* protein ESAT-6 is a potent activator of the NLRP3/ASC inflammasome. *Cell Microbiol* 12:1046–1063.
30. Carlsson F, et al. (2010) Host-detrimental role of Esx-1-mediated inflammasome activation in mycobacterial infection. *PLoS Pathog* 6:e1000895.
31. Hiesinger PR, et al. (2005) The v-ATPase V0 subunit a1 is required for a late step in synaptic vesicle exocytosis in Drosophila. *Cell* 121:607–620.
32. Li G, Alexander EA, Schwartz JH (2003) Syntaxin isoform specificity in the regulation of renal H+-ATPase exocytosis. *J Biol Chem* 278:19791–19797.
33. Clemens DL, Horwitz MA (1996) The *Mycobacterium tuberculosis* phagosome interacts with early endosomes and is accessible to exogenously administered transferrin. *J Exp Med* 184:1349–1355.
34. Peplowska K, Markgraf DF, Ostrowicz CW, Bange G, Ungermann C (2007) The CORVET tethering complex interacts with the yeast Rab5 homolog Vps21 and is involved in endo-lysosomal biogenesis. *Dev Cell* 12:739–750.
35. Wurmser AE, Sato TK, Emr SD (2000) New component of the vacuolar class C-Vps complex couples nucleotide exchange on the Ypt7 GTPase to SNARE-dependent docking and fusion. *J Cell Biol* 151:551–562.
36. Nickerson DP, Brett CL, Merz AJ (2009) Vps-C complexes: Gatekeepers of endolysosomal traffic. *Curr Opin Cell Biol* 21:543–551.
37. Takeda K, et al. (2008) The vacuolar V1/V0-ATPase is involved in the release of the HOPS subunit Vps41 from vacuoles, vacuole fragmentation and fusion. *FEBS Lett* 582: 1558–1563.
38. Plemel RL, et al. (2011) Subunit organization and Rab interactions of Vps-C protein complexes that control endolysosomal membrane traffic. *Mol Biol Cell* 22:1353–1363.
39. Sun J, et al. (2007) *Mycobacterium bovis* BCG disrupts the interaction of Rab7 with RILP contributing to inhibition of phagosome maturation. *J Leukoc Biol* 82: 1437–1445.
40. Vergne I, Constant P, Lanéelle G (1998) Phagosomal pH determination by dual fluorescence flow cytometry. *Anal Biochem* 255(1):127–132.
41. Bernardo J, Long HJ, Simons ER (2010) Initial cytoplasmic and phagosomal consequences of human neutrophil exposure to *Staphylococcus epidermidis*. *Cytometry A* 77:243–252.

Supporting Information

Wong et al. 10.1073/pnas.1109201108

SI Materials and Methods

Mtb Strains and Growth Conditions. Parental WT H37Rv, the Δ*ptpA* deletion mutant strains, and the complemented strains were grown as described previously (1). For complementation of Δ*ptpA*, DNA sequences encoding WT PtpA or mutant PtpA proteins under the control of the native promoter, or the *hps60* promoter, were cloned into the pKP201 integrative vector. The Δ*ptpA* strain was cotransformed with the resulting plasmids and pBS*int*, a nonreplicating plasmid that provides integrase *in trans*. Transformants were selected on 7H11 medium with 50 μg/mL hygromycin.

In Vitro Kinase Assay and Phosphoamino Acid Analysis. In vitro kinase assay and phosphoamino acid analysis were performed as described previously (1).

Phosphatase Activity Assay. Phosphatase activity assay was performed as described previously (2).

Antibodies. Affinity-purified rabbit polyclonal anti-VPS33B and rabbit polyclonal anti-subunit E (ATP6V1E1) were purchased from Proteintech Group. Affinity-purified rabbit polyclonal anti-subunit H (ATP6V1H) and rabbit polyclonal anti-subunit B (ATP6V1B) were purchased from Santa Cruz Biotechnology. Affinity-purified rabbit polyclonal anti-VPS18 was purchased from Applied Biological Materials. Affinity-purified mouse polyclonal anti-subunit H was purchased from Sigma-Aldrich. 4G10 anti-phosphotyrosine antibody was purchased from Millipore. Rabbit anti-protein tyrosine phosphatase (PtpA) was described previously (1, 2). Specificity of the commercial antibodies was tested with FACS analysis, Western blot analysis, and an immunostaining control experiment (Fig. S7).

Double Immunofluorescence Staining. Infected THP-1 macrophages on coverslips were fixed with 2.5% paraformaldehyde for 30 min at 37 °C. The fixed macrophages were then washed with PBS before permeabilization with 0.2% saponin and blocking with 1% normal goat serum in PBS for 30 min at room temperature. Double immunostaining was performed sequentially with rabbit anti-VPS33B at 10 μg/mL in 0.2% saponin and 1% normal goat serum and mouse anti-subunit H at 10 μg/mL in 0.2% saponin and 1% normal goat serum. Texas Red-conjugated goat anti-rabbit IgG (Invitrogen) and Alexa Fluor 488-conjugated goat anti-mouse IgG, both of which are highly cross-adsorbed to minimize cross-reactivity, were used at a dilution of 1:1,000.

In Vitro PtpA Secretion Analysis. The DNA encoding His-tagged PtpA under the control of the *hsp60* promoter was cloned into the pMV261 vector. The resulting plasmid was transformed into the WT H37Rv *Mycobacterium tuberculosis* (Mtb) strain, and the transformed strain was grown to an OD_{600} = 0.8 in 50 mL of Sauton's medium supplemented with 0.05% Tween-80. Covalent labeling of bacteria with pHrodo and Alexa Fluor 488 was performed according to manufacturer's protocol. The unlabeled and labeled bacteria were than reinoculated into 50 mL of fresh Sauton's medium with 0.05% Tween-80 and grown for 48 h at 37 °C. The culture filtrate proteins were then harvested and precipitated with 10% TCA and 0.1% SDS as described before (3). The samples were resolved on 10% SDS/PAGE, and PtpA secretion into the culture supernatant was analyzed with Western blotting using rabbit anti-PtpA and mouse anti–His-tag.

Phagosomal pH Measurement of THP-1 Macrophages Infected with Mtb. THP-1 macrophages were seeded on six-well plates (1.0×10^6) with 40 ng/mL 12-phorbol 13-myristate acetate (PMA). Mtb strains were first labeled with 20 μM pHrodo succinimidyl ester (SS; Invitrogen) at 37 °C for 1 h. The bacteria were washed with 7H9 supplemented with 0.05% Tween-80 three times before being labeled with 25 μg/mL Alexa Fluor 488 carboxylic acid SS (Invitrogen). The bacteria were then washed and opsonized with human serum. The THP-1 macrophages were then infected with the labeled Mtb at a multiplicity of infection (MOI) of 10:1 for 2 h at 37 °C with 5% CO_2. Noninternalized bacteria were washed away, and the infection was incubated for another 2 h at 37 °C with 5% CO_2. For pH calibration, the infected cells were incubated in 10 mM phosphate-citrate buffer with predetermined pH (5.0–8.0; *Materials and Methods*). The cells were then washed, scraped off the plate, and fixed with 2.5% paraformaldehyde. pHrodo is stable after fixation with paraformaldehyde (4). The fixed cells were then analyzed with FACS on FACSCalibur (BD Bioscience) and FlowJo 8.7 software. Color compensation was performed to prevent signal overlapping. Mean fluorescence intensities of pHrodo and Alexa Fluor 488 were used to calculate pHagosomal pH.

Single Transfection of THP-1 Macrophages. THP-1 macrophages were transfected with the mammalian pEGFP vector harboring the GFP-tagged PtpA constructs using the Nucleofector Cell Line Nucleofector Kit V (Lonza) according to the manufacturer's protocol. Transfected macrophages were seeded in 96-well plates in the presence of 40 ng/mL PMA and incubated at 37 °C with 5% CO_2. Expression of GFP-tagged proteins was measured 12 h after transfection with spectrofluorometry (emission 535 nm).

Phagocytosis Assay. THP-1 macrophages were transfected and seeded as noted previously. *Escherichia coli* was labeled with 50 μg/mL Alexa Fluor 350 carboxylic acid SS (Invitrogen) at 37 °C for 1 h. The bacteria were then washed with PBS and opsonized with human serum. The transfected cells were infected with the labeled *E. coli* at a MOI of 10:1. Phagocytosis was synchronized as described previously (5). Noninternalized bacteria were washed away after incubation at 37 °C for 15 min, and phagocytosis was measured by spectrofluorometry.

Phagosomal pH Measurement of THP-1 Macrophages Infected with *E. coli*. Transfection, *E. coli* labeling with pHrodo SS, and Alexa Fluor 350 carboxylic acid SS and THP-1 infection were performed as described previously. For pH calibration, the infected cells were incubated in 10 mM phosphate-citrate buffer with predetermined pH (5.0–8.0) (*Materials and Methods*) after noninternalized bacteria were washed away. pHrodo fluorescence (emission 620 nm) and Alexa Fluor 350 fluorescence (emission 460 nm) were measured simultaneously in the Fusion-α HT microplate reader (Perkin-Elmer).

FACS Analysis of Antibodies Specificity. H37Rv Mtb harboring a plasmid construct for the expression of DsRed was grown to OD_{600} = 0.8 in 7H9 medium supplemented with 10% oleic acid-albumin-dextrose-catalase and 0.05% Tween-80. The bacteria were washed three times with 7H9 supplemented with 0.05% Tween-80 (7H9T), and 1.0×10^8 was resuspended in 100 μL 7H9T. The indicated primary antibodies were added to the bacteria at a final concentration of 5 μg/mL and incubated at 37 °C with shaking for 1 h. The bacteria were then washed three times with 7H9T and incubated with either Alexa Fluor-conjugated goat

anti-rabbit IgG (Invitrogen) or Alexa Fluor 488 goat anti-mouse IgG (Invitrogen) secondary antibodies at a dilution of 1:1,000 for 1 h at 37 °C with shaking. The bacteria were then washed with 7H9T and fixed with 2.5% paraformaldehyde for 30 min at 37 °C. The fixed bacteria were subjected to FACS analysis with FACS-Calibur (BD Bioscience) for antibody binding. Expression of DsRed in Mtb allows specific gating to distinguish the bacterial population from background noise signal. Color compensation was performed to prevent signal overlapping.

Coimmunoprecipitation. THP-1 cells were infected as above, harvested at 4 h or 24 h postinfection, and lysed in buffer containing Protease Inhibitor Mixture (Roche). Lysates were centrifuged to separate the soluble and insoluble fractions. Soluble fractions were used for coimmunoprecipitation. Briefly, rabbit anti-VPS33B or rabbit anti-subunit H was added to 2 mg or 4 mg of soluble lysate (1:100 dilution), and the mixture was incubated at room temperature for 1 h. Affi-Gel protein A agarose resin (Bio-Rad) was blocked with 0.5% BSA, washed with PBS, then added to the lysate and incubated at room temperature with shaking for 1 h to bind to the antibody–antigen complexes. The resin was then washed with PBS, and SDS sample buffer was added. The resulting samples were resolved on SDS-PAGE and transferred onto a nitrocellulose membrane for Western blot analysis with the indicated primary antibodies. Protein A-HRP was used as the secondary detection reagent. For Western blot analysis with antiphosphotyrosine 4G10, recombinant VPS33B protein was phosphorylated in kinase buffer as previously described (1) with 0.5 μM ATP and probed as a control along with the immunoprecipitated samples.

Double Transfection of THP-1 Macrophages. The genes encoding subunit H and VPS33B were cloned into pEGFP-N1 and pDsRed2-N1 vectors (Clontech), respectively. THP-1 cells were seeded onto coverslips in 24-well plates at a density of 1 million cells per well and differentiated with PMA at 20 ng/mL overnight. Transfection was carried out by magnetofection using PolyMAG reagent (Chemicell). In brief, 1.5 μg of each DNA construct was mixed with 1 μL of PolyMAG reagent in a volume of 200 μL serum-free and supplement-free RPMI 1640 (Sigma). This mixture was incubated for 15 min at room temperature and then added to each well containing 300 μL of RPMI medium 1640 supplemented with 10% FBS, 1% L-glutamine (StemCell). Thereafter, the 24-well plate was placed upon a magnetic plate and incubated for 30 min at 37 °C. The magnet was then removed and cells were incubated overnight for expression of the fluorescent proteins.

1. Bach H, Papavinasasundaram KG, Wong D, Hmama Z, Av-Gay Y (2008) *Mycobacterium tuberculosis* virulence is mediated by PtpA dephosphorylation of human vacuolar protein sorting 33B. *Cell Host Microbe* 3:316–322.
2. Cowley SC, Babakaiff R, Av-Gay Y (2002) Expression and localization of the *Mycobacterium tuberculosis* protein tyrosine phosphatase PtpA. *Res Microbiol* 153:233–241.
3. Joshi B, et al. (2010) A simple and rapid method of sample preparation from culture filtrate of *M. tuberculosis* for two-dimensional gel electrophoresis. *Braz J Microbiol* 41: 295–299.
4. Miksa M, Komura H, Wu R, Shah KG, Wang P (2009) A novel method to determine the engulfment of apoptotic cells by macrophages using pHrodo succinimidyl ester. *J Immunol Methods* 342(1-2):71–77.
5. Iyer SS, Barton JA, Bourgoin S, Kusner DJ (2004) Phospholipases D1 and D2 coordinately regulate macrophage phagocytosis. *J Immunol* 173:2615–2623.
6. Lesk VI, Sternberg MJ (2008) 3D-Garden: A system for modelling protein-protein complexes based on conformational refinement of ensembles generated with the marching cubes algorithm. *Bioinformatics* 24:1137–1144.

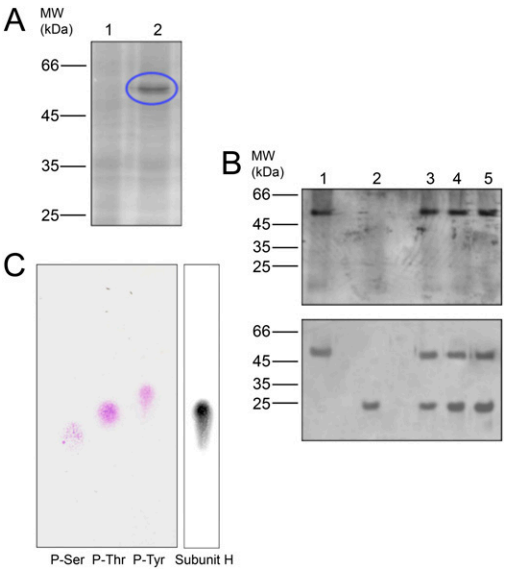

Fig. S1. In vitro analysis of subunit H and PtpA interaction. (*A*) Recombinant PtpA pulled down V-ATPase subunit H from the THP-1 cell lysate. Recombinant His-tagged PtpA proteins were used as a bait to pull down target proteins from THP-1 human macrophages lysates. Lane 1: THP-1 cell lysate alone. Lane 2: THP-1 cell lysate incubated with His-tagged WT PtpA protein. PtpA pulled down V-ATPase subunit H (blue circle). MALDI-TOF mass spectrometry was used to analyze the captured proteins (1). (*B*) Phosphorylated subunit H is not a catalytic substrate of PtpA. (*Upper*) Phosphorimage of subunit H recombinant proteins phosphorylated with $\gamma[^{32}P]$ATP and incubated with increasing concentration of PtpA recombinant proteins. Lane 1, subunit H alone; lane 2, PtpA alone; lane 3, subunit H and PtpA (1:1 molar ratio); lane 4, subunit H and PtpA (1:2 molar ratio); lane 5, subunit H and PtpA (1:3 molar ratio). (*Lower*) Silver-stained SDS/PAGE of the corresponding gel. (*C*) Phosphoamino acid analysis shows subunit H is Thr phosphorylated. Phosphoamino acid analysis was performed as described previously (1). Phospho-serine (P-Ser), 0.44; phospho-threonine (P-Thr), 0.49; phospho-tyrosine (P-Tyr), 0.55. Subunit H, 0.50.

1. Bach H, Papavinasasundaram KG, Wong D, Hmama Z, Av-Gay Y (2008) *Mycobacterium tuberculosis* virulence is mediated by PtpA dephosphorylation of human vacuolar protein sorting 33B. *Cell Host Microbe* 3:316–322.

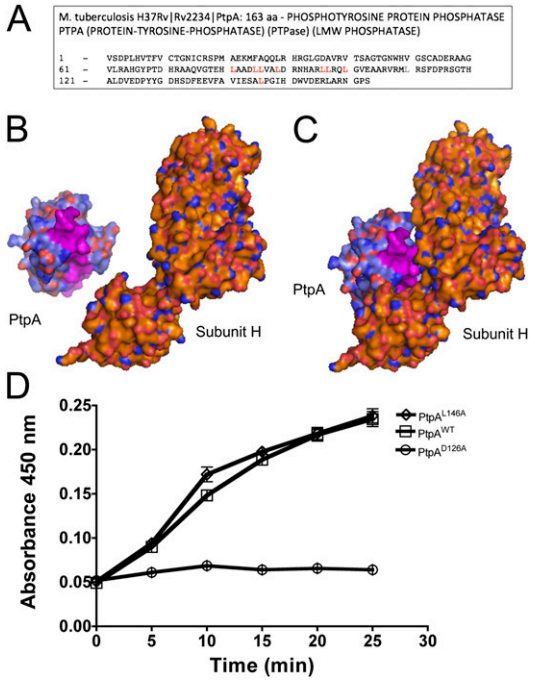

Fig. S2. PtpA^{L146A} is defective in binding subunit H. (*A*) Site-directed mutagenesis of dileucine motifs and leucine residues in PtpA. Highlighted amino acids are the residues mutated and tested. Leu146Ala mutation creates a catalytically active mutant PtpA that does not interact with subunit H of the V-ATPase. (*B*) Computer-generated model of PtpA complexed with the V-ATPase subunit H based upon 3D-Garden macromolecular docking analysis (1) of the crystal structure of Mtb PtpA (PDB accession no. 1U2P) and yeast V-ATPase subunit H (PDB accession no. 1HO8). Surface representation of PtpA and subunit H as separated molecules. The C-terminal α-helix of PtpA is colored in magenta. Leu146Ala mutation on PtpA likely alters the C-terminal α-helix, leading to the defective binding. (*C*) Computer prediction of PtpA binding on subunit H with the C-terminal α-helix of PtpA docking onto the cleft region between the N-terminal and C-terminal domain of subunit H. (*D*) PtpA^{L146A} remains catalytically active with similar kinetics as the WT enzyme despite point mutation on its C-terminal α-helix. p-nitrophenyl phosphate is used as a chromogenic substrate to detect phosphatase activity of PtpA as described previously (2). The reactions were analyzed in a spectrophotometer for absorbance at 450 nm.

1. Lesk VI, Sternberg MJ (2008) 3D-Garden: A system for modelling protein-protein complexes based on conformational refinement of ensembles generated with the marching cubes algorithm. *Bioinformatics* 24:1137−1144.
2. Cowley SC, Babakaiff R, Av-Gay Y (2002) Expression and localization of the *Mycobacterium tuberculosis* protein tyrosine phosphatase PtpA. *Res Microbiol* 153:233−241.

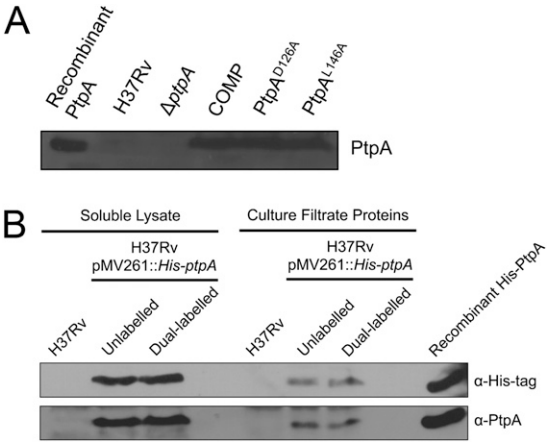

Fig. S3. Western blot analysis of PtpA expression in complemented ΔptpA strains and in vitro PtpA secretion using α-PtpA antibodies. (*A*) A weak band corresponding to PtpA expression is observed for the parental H37Rv as expected. ΔptpA strains complemented with WT ptpA (COMP), ptpA^{D126A}, or ptpA^{L146A} shows clear expression of PtpA proteins. Recombinant PtpA was used as a positive control. No expression was observed for the ΔptpA strain. (*B*) Covalent labeling of the bacteria with pHrodo and Alexa Fluor 488 does not affect PtpA secretion as shown by the prominent bands corresponding to His-tagged PtpA in the culture filtrate. Soluble lysates from the bacteria were analyzed to ensure expression of His-tagged PtpA. Recombinant PtpA was used as a positive marker control.

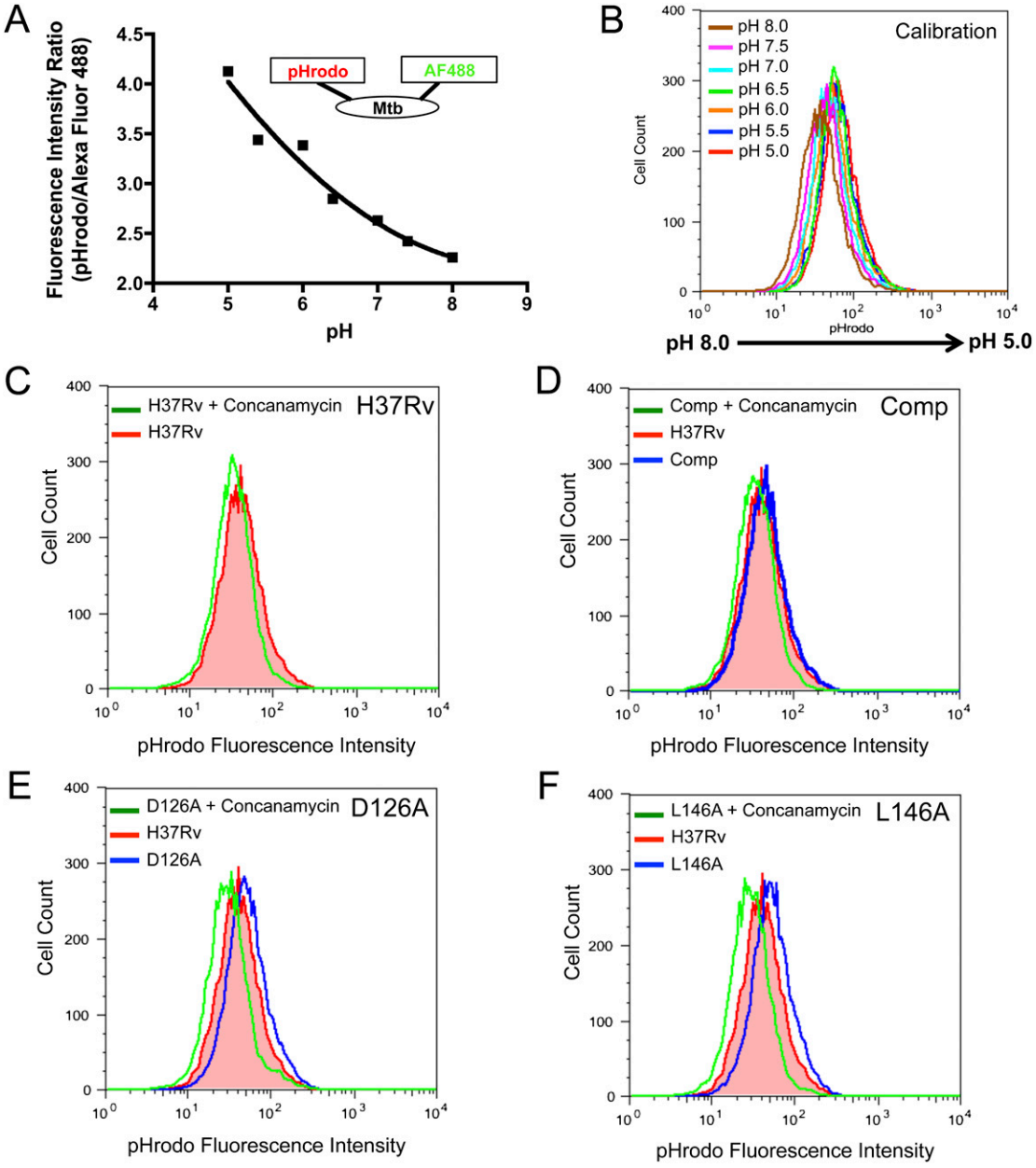

Fig. S4. Calibration of THP-1 phagosomal pH during Mtb infection with FACS. (*A*) Calibration curve of phagosomal pH in THP-1 macrophages infected with Mtb, dual labeled with pHrodo and Alexa Fluor 488. The fluorescence intensity ratios of the fluorescence probes were calculated and plotted for each pH. (*B*) Overlaid FACS histograms of the pHrodo fluorescence intensities of Mtb phagosomes at precalibrated pH (5.0–8.0). (*C*–*F*) Overlaid FACS histograms of pHrodo fluorescence intensities of THP-1 macrophages infected with the indicated Mtb strains. (*C*) Parental H37Rv. (*D*) Δ*ptpA* complemented with the WT *ptpA* gene. (*E*) Δ*ptpA* complemented with the mutant $ptpA^{D126A}$ gene. (*F*) Δ*ptpA* complemented with the mutant $ptpA^{L146A}$ gene.

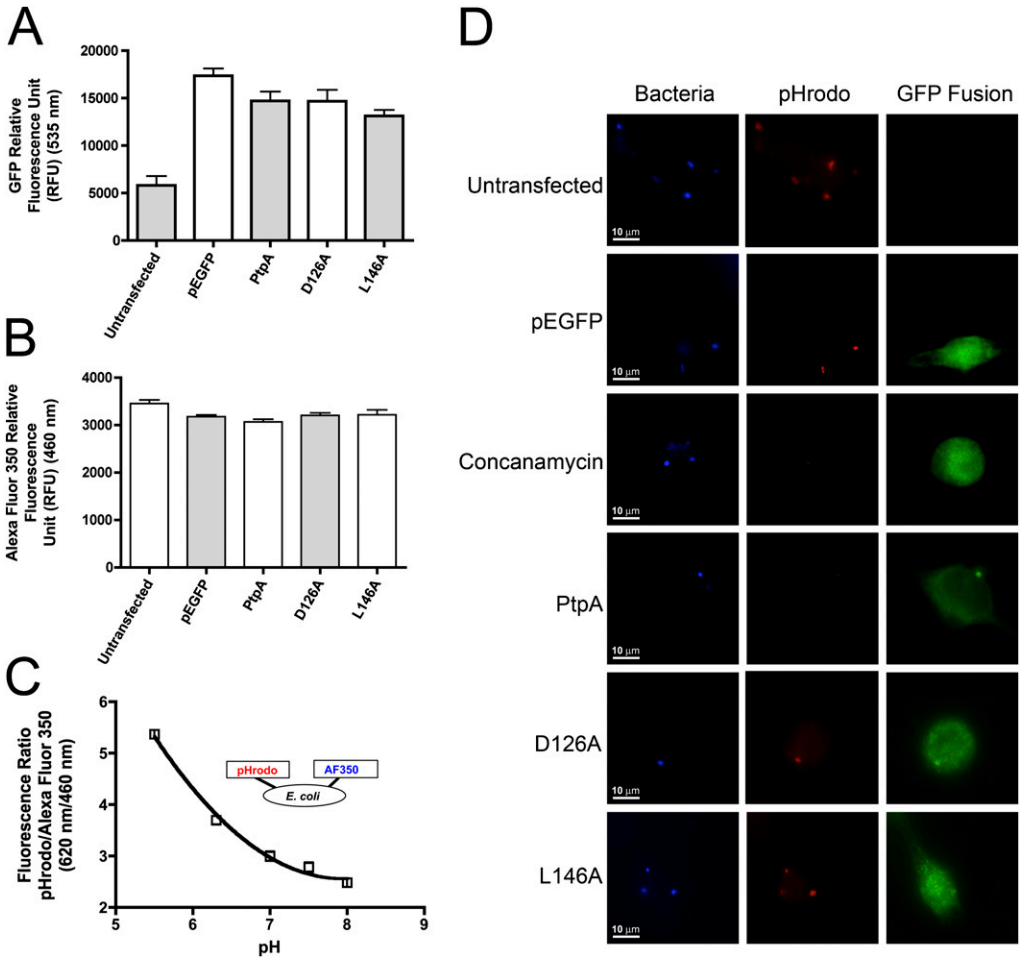

Fig. S5. Measurement of phagosomal pH in transfected THP-1 infected with *E. coli*. (*A*) Expression of GFP-tagged WT and mutant PtpA proteins were assessed by measurement of GFP fluorescence (emission 535 nm) in transfected THP-1 macrophages. Similar levels of expression were found for the WT and mutant proteins. Untransfected THP-1 serves as a negative control, and THP-1 transfected with the pEGFP vector was used as a positive control. (*B*) Phagocytosis of *E. coli* labeled with Alexa Fluor 350 by THP-1 macrophages was not affected by transfection and expression of GFP-tagged WT and mutant PtpA proteins. There was no difference in the level of phagocytosis of THP-1 transfected cells with untransfected cells as shown by the similar levels of Alexa Fluor 350 fluorescence (emission 460 nm). (*C*) Calibration of THP-1 phagosomal pH during *E. coli* infection with spectrofluorometry. The fluorescence ratios of pHrodo (emission 620 nm) and Alexa Fluor 350 (emission 460 nm) were plotted for each pH to generate the calibration curve of phagosomal pH in THP-1 macrophages infected with *E. coli* dual labeled with the pH-sensitive pHrodo and pH-insensitive Alexa Fluor 350 dyes. (*D*) Separate digital confocal microscopy fluorescent images of transfected THP-1 macrophages infected with dual-labeled *E. coli*. Green, expression of GFP or GFP-tagged PtpA constructs; red, pHrodo fluorescence in acidified phagosomes; blue, Alexa Fluor 350-labeled *E. coli*. Localization of GFP-PtpA to the phagosomes can be observed.

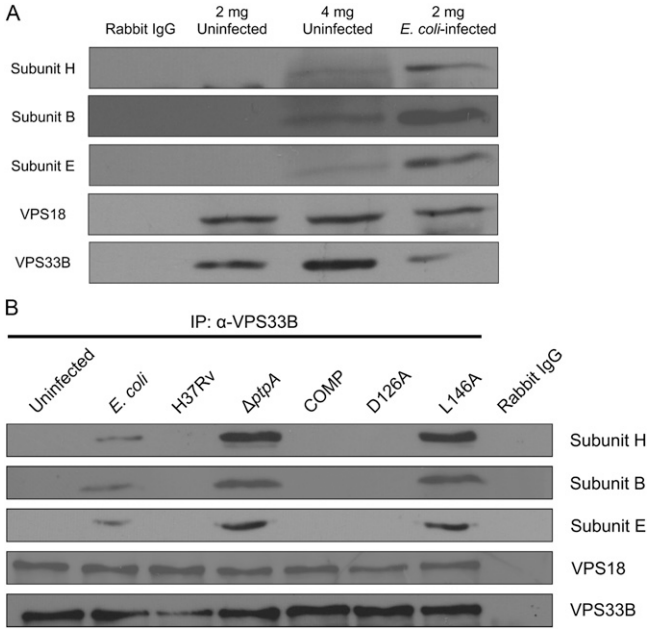

Fig. S6. Coimmunoprecipitation of V-ATPase subunits with class C VPS. (*A*) V-ATPase subunits (H, B, and E) can be captured with VPS33B and VPS18 from uninfected THP-1 macrophages when immunoprecipitation was performed using 4 mg of soluble lysate. The interaction was not detected when 2 mg lysate was used. Prominent bands corresponding to V-ATPase subunits can be pulled down from 2 mg lysate from *E. coli*-infected THP-1 macrophages. (*B*) Mtb disruption of V-ATPase interaction with class C VPS can be observed 24 h postinfection. IP was performed with either rabbit IgG or anti-VPS33B (α-VPS33B) using 2 mg of soluble lysate from THP-1 macrophages infected for 24 h. For the Δ*ptpA* and Δ*ptpA* complemented with $PtpA^{L146A}$ strains, V-ATPase interaction with class C VPS remains up-regulated 24 h postinfection, suggesting continued delivery of lysosomal contents and killing of the bacteria in the phagosomes.

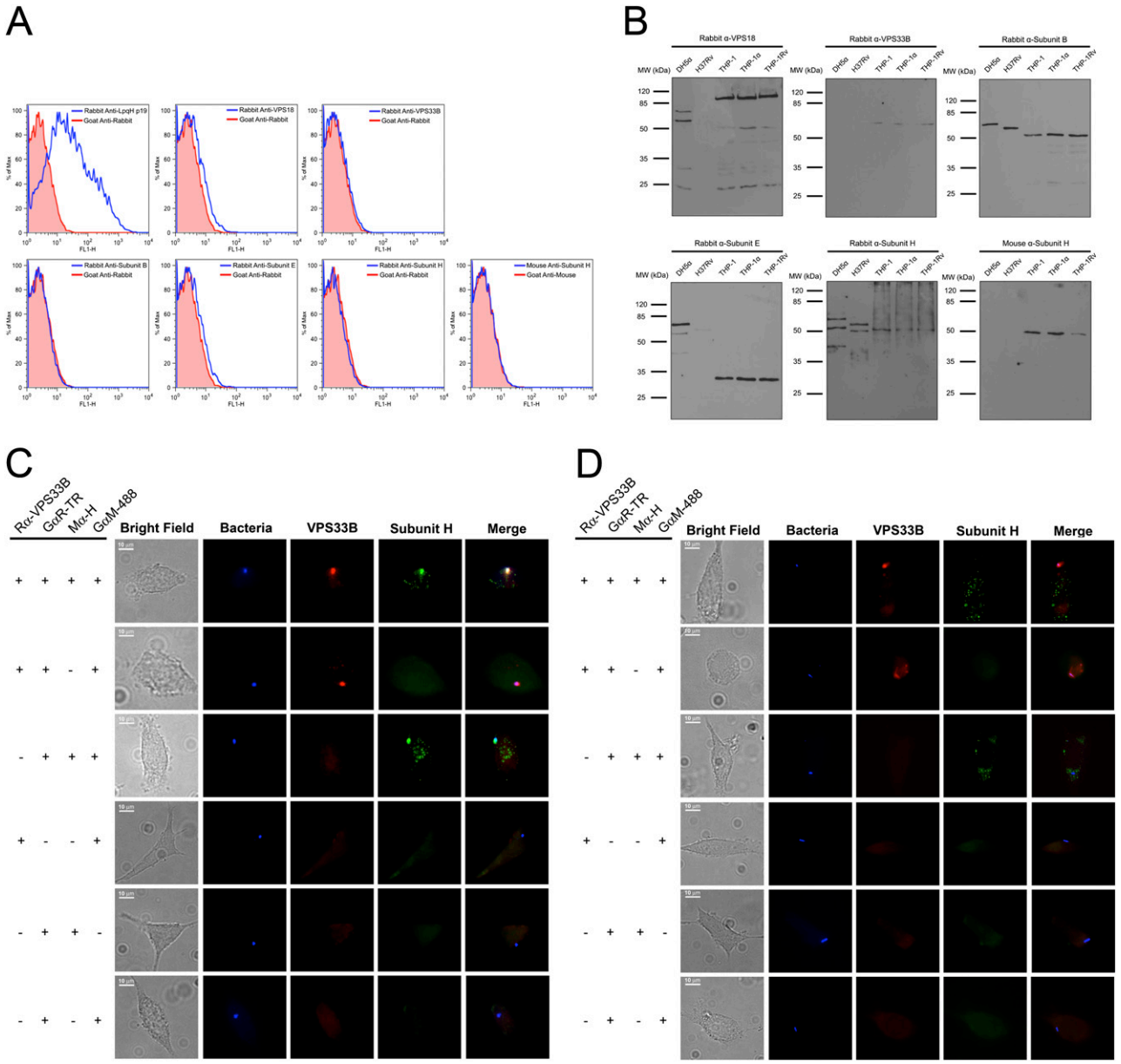

Fig. S7. Analysis of antibodies' specificity. (*A*) FACS analysis of the ability of indicated antibodies to nonspecifically recognize extracellular components of Mtb. None of the tested antibodies showed significant binding to the bacteria. Rabbit anti-LqpH (19-kDa lipoprotein that is known to be present on the Mtb cell wall) was used as a positive control. Western blot analysis of antibodies specificity with soluble lysates from *E. coli* DH5α, Mtb H37Rv, THP-1, THP-1 infected with *E. coli* DH5α (THP-1α), and THP-1 infected with Mtb H37Rv (THP-1Rv). A total of 25 μg of each lysate was resolved on SDS/PAGE and probed with the indicated antibodies. The tested antibodies showed specific detection of the target proteins with minimal nonspecific background signal. (*C* and *D*) An immunostaining control experiment was performed to examine potential cross-reactivity among the secondary antibodies. Rabbit anti-VPS33B (Rα-VPS33B) and mouse anti-subunit H (Mα-H) were used as primary antibodies. Texas Red-conjugated goat anti-rabbit IgG and Alexa Fluor 488-conjugated goat anti-mouse IgG were used as secondary antibodies. Fluorescent signal was only detected when the correct pair of primary and secondary antibodies was used. The secondary antibodies do not react with primary antibodies from another species, demonstrating the specificity of the secondary antibodies for double immunofluorescence staining. (*C*) THP-1 macrophages infected with Alexa Fluor 350-labeled *E. coli*. (*D*) THP-1 macrophages infected with Alexa Fluor 350-labeled H37Rv Mtb.

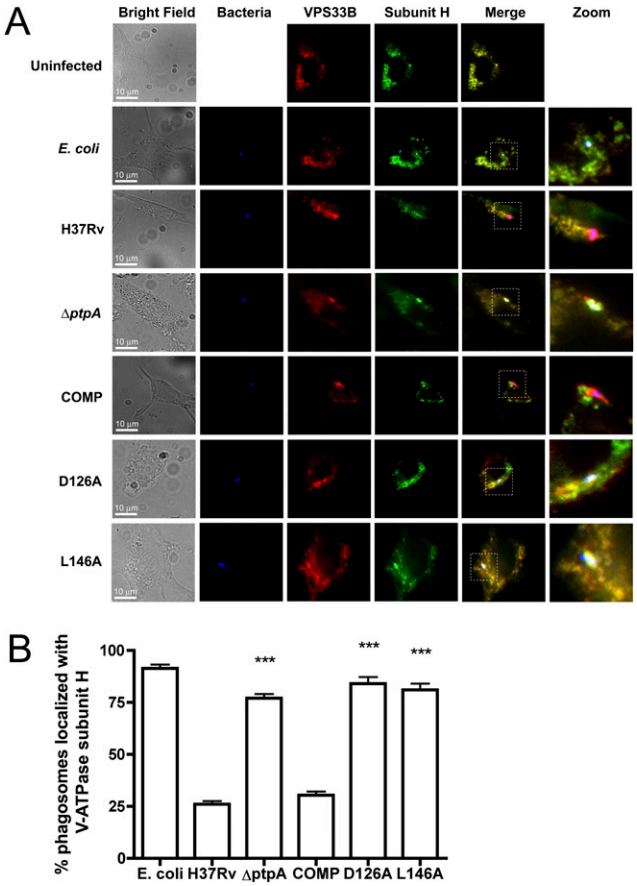

Fig. S8. Confocal microscopy of THP-1 macrophage doubly transfected with GFP-subunit H and DsRed2-VPS33B. The transfected macrophages were infected with *E. coli* or indicated Mtb strains, and the localization of subunit H and VPS33B was directly visualized. V-ATPase was excluded from the Mtb phagosome in macrophages infected with the WT strain, and the Δ*ptpA* phagosome acquired V-ATPase. The phagosomes of the binding-defective $PtpA^{L146A}$-expressing strain also failed to exclude host V-ATPase. (*B*) Quantification of the confocal data shown in *A*. ***$P < 0.001$ (significant difference compared with H37Rv by Student *t* test).

Table S1. Phagosomal pH of Mtb strains in THP-1 macrophages

	pHrodo MFI	Alexa Fluor 488 MFI	Fluorescence ratio (pHrodo/AF488)	pH	SE	*P* value
WT	42.23	15.40	2.74	6.73	0.38	NA
Δ*ptpA*	47.53	14.17	3.36	5.78	0.04	0.012
Complement	44.20	15.15	2.92	6.42	0.01	NS
D126A	50.87	14.47	3.52	5.58	0.09	0.0067
L146A	49.17	13.90	3.54	5.55	0.09	0.0063

AF488, Alexa Fluor 488; MFI, mean fluorescence intensity; N/A, not applicable; NS, not significant.